# On the Conversion of InP Clusters to Quantum Dots.

Max R. Friedfeld, Dane A. Johnson, Brandi M. Cossairt*

*Department of Chemistry, University of Washington, Seattle, Washington 98195-1700, United States*

**ABSTRACT:** Understanding and deconvoluting the different mechanisms involved in the synthesis of nanomaterials is necessary to make uniform materials with desirable function. In this study, in-situ spectroscopic methods were used to study exchange reactions at the surface of indium phosphide clusters, revealing that the cluster surface lacks significant dynamics on the NMR time-scale at room temperature. The exchange of surface carboxylate ligands can be induced at elevated temperatures and with the addition of carboxylic acid and indium carboxylate. These studies suggest that carboxylate may be a key ingredient in promoting cluster dissolution to larger nanostructures. Toward this end, the evolution of InP clusters was examined by in situ UV-Vis spectroscopy, revealing cluster dissolution and re-nucleation that is dramatically dependent on the concentration of carboxylate. In addition to the concentration of exogenous ligands, the rate of particle growth and final product distribution was dependent on temperature and initial cluster concentration. These results, taken together, suggest a mechanism of cluster evolution involving cluster dissociation to form multiple reactive monomer species that re-nucleate and grow to larger nanomaterials. Non-productive monomer degradation is observed in the lower temperature regime (< 200 °C), suggesting a critical temperature threshold for efficient cluster to quantum dot conversion.

## INTRODUCTION

Understanding the formation mechanisms of colloidal semiconducting nanocrystals is essential in developing uniform materials with desirable physical properties and photophysical function. As more work has focused on this issue, it has become clear that classical nucleation theories that describe the formation of certain lattices (e.g., highly ionic lattices like AgCl and NaCl, and elemental ones including Ag and S clusters) are not sufficient to describe the nucleation of many classes of semiconducting nanoparticles, or colloidal quantum dots (QDs).[1,2,3,4] The range of covalency in different semiconducting materials, numerous precursors and other reaction conditions available in solution-processible materials, and advances in spectroscopic observation have all enabled a more nuanced and complete description of the nucleation mechanisms for these nanomaterials. With certain systems, multiple mechanisms can operate concurrently depending on reaction conditions, while with others, temporally distinct mechanisms exist, enabling isolation of intermediate clusters or allowing for distinct nucleation and ripening stages to be observed.

The intermediacy of so-called "magic-sized" clusters, MSCs, has been implicated in the synthesis of many semiconducting nanomaterials, including II-VI, IV-VI, and III-V QDs.[5] The conversion mechanisms of these molecularly well-defined and atomically precise clusters to QDs has been demonstrated to occur by two distinct mechanism types: (1) monomer-driven growth and (2) cluster assembly. Monomer-driven growth occurs when a reservoir of monomers derived from cluster dissolution, or generated from separate molecular precursors, react with clusters to form larger nanomaterials. Monomer-driven growth can occur through one of three pathways, (1) monomer deposition onto MSC seeds,[6,7,8] (2) quantized cluster growth (also called Ostwald staging), [9,10,6,11,12] or (3) complete dissolution/re-nucleation for each MSC population.[13,14,15]

Cluster assembly or oriented attachment, wherein clusters aggregate together to make larger nanomaterial without a monomer reservoir, has been demonstrated with II-VI nanowires,[16,17,18] ZnS nanorods,[19] and PbS nanocrystals.[20,21] Differentiating between these mechanisms is not straightforward and requires a suite of corroborating experiments, including adding and removing monomer reservoirs and correlating nanomaterial size dimensions to initial cluster dimensions.[5,22,23] The use of in-situ spectroscopic techniques (e.g., UV-Vis, small- and wide-angle X-ray scattering, solution TEM), while rarely used to study MSC conversion mechanisms, would be useful in characterizing reactive intermediates and observing real-time changes without perturbing the reaction system.

Such in-situ spectroscopic techniques have been used in studying QD growth from molecular precursors, but ex-situ techniques (e.g., reaction aliquots for UV-Vis, TEM) are far more prevalent.[24,25] The growth of CdSe nanocrystals from precursors was first studied independently by Peng[26] and Reiss[27] using in-situ UV-Vis spectroscopy with millisecond resolution, revealing smooth progression to larger and larger QDs while maintaining low polydispersity. In another CdSe system, in-situ small- and wide-angle X-ray scattering was used to monitor the nucleation and growth pathways, demonstrating that the lamellar structure of the precursor dissolves prior to cluster formation.[28] Microfluidic devices have been developed to provide millisecond resolution in the nucleation and growth of PbS,[29] and millisecond stop-flow UV-Vis has been used in studying the early growth stages of ZnS,[30] and AgS.[31] In-situ observation techniques have also been used in studying other II-VI[32,33,34,35,36] and metal nanoparticle[37,38,39,40] nucleation and growth.

The role of MSCs in the nucleation and growth mechanism of InP QDs has been intensely studied due to its emergence as an important material for emissive display and lighting applications.[41,42] We were interested in applying in-situ spectroscopic techniques to study the conversion of InP MSCs to larger nanomaterials in order to deduce the condition-dependent mechanism(s) by which MSCs convert to larger nanostructures. During early stages of InP QD synthesis from indium carboxylate, $In(O_2CR)_3$, and tris(trimethylsilyl)phosphine, $P(SiMe_3)_3$, a meta-stable phase of InP is observed.[43,44] Lowering the reaction temperature to 100 °C enables isolation of a magic-sized cluster as a monodisperse phase of InP characterized by an excitonic feature centered at 386 nm and a powder XRD pattern distinct from bulk and nanocrystalline zincblende InP.[35] Modification of the carboxylate ligand to the more rigid phenylacetate ligand, $[O_2CCH_2Ph]^-$ enables the isolation and single-crystal X-ray structure determination of the InP MSC, identified with the same absorption fingerprint and a chemical formula of $In_{37}P_{20}(O_2CCH_2Ph)_{51}$.[45] The molecular structure of the InP MSC revealed a number of interesting features including a non-stoichiometric charged $[In_{21}P_{20}]^{3+}$ core surrounded by 16 $In^{3+}$ ions and 51 carboxylate $[O_2CCH_2Ph]^-$ ligands in exclusively bidentate and predominantly bridging binding modes. Furthermore, the inorganic $[In_{37}P_{20}]$ core is characterized by low pseudo-$C_{2v}$ symmetry, a deviation from the expected tetrahedral structure of bulk zincblende InP. The InP MSC was demonstrated to serve as a single-source precursor for InP QDs upon performing a hot injection of MSCs into squalane at 400 °C,[43] however little is currently known about the condition dependence of this reaction or how to control particle morphology and other structural variables.

Based on our initial studies of this system and the body of work that has been reported on cluster conversion mechanisms, we can propose several general pathways by which MSCs can convert to InP QDs, Scheme 1. When subjected to elevated temperatures, the MSC may undergo dissolution to a mixture of monomers and indium carboxylate that could either result in QD nucleation directly (path 1) or through monomer addition to remaining MSC (path 2). Additionally, a templated, or seeded, growth mechanism (path 3) could be relevant, similar to what was previously implicated in the low temperature, kinetically controlled growth of QDs from MSCs via slow addition of $P(SiMe_3)_3$.[46] Further complicating these scenarios is that at different points in the reaction and with slight changes to the reaction conditions (i.e. – temperature, ligand concentration), different monomer species may be mechanistically relevant.

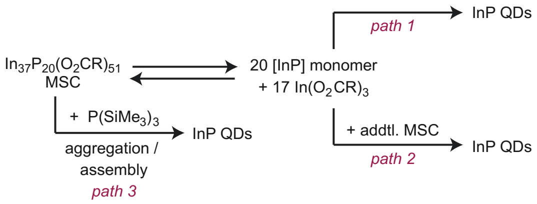

**Scheme 1. General mechanisms describing the conversion of MSCs to QDs.**

In this report we use in-situ spectroscopic methods ($^{13}$C-NMR, UV-Vis) to study the surface chemistry and photophysical evolution that accompany the InP MSC to QD conversion process. Ultimately we seek to elucidate the microscopic mechanisms by which the cluster converts to QDs and reveal the complex landscape of monomer species that are relevant in these processes.

## RESULTS AND DISCUSSION

### Part 1. $^{13}$C NMR studies on isotopically labeled clusters.

To study the role of surface chemistry on the cluster conversion process, an isotopically labeled InP MSC, $In_{37}P_{20}(O_2{}^{13}CCH_2Ph)_{51}$, *$^{13}$C*-MSC, was synthesized and studied via $^{13}$C-NMR spectroscopy. This cluster was prepared from $In(OAc)_3$, isotopically-pure phenylacetic acid, $PhCH_2{}^{13}CO_2H$, and $P(SiMe_3)_3$, in a manner analogous to the synthesis of the myristate- and the phenylacetate-ligated MSCs.[43,45] The absorbance properties of the labeled MSC (*$^{13}$C*-MSC) are essentially identical to the natural-abundance cluster (Figure S1), enabling the use of *$^{13}$C*-MSC to study the acid-induced displacement of surface carboxylate.

The room temperature $^{13}$C NMR spectrum of *$^{13}$C*-MSC displays a complex set of carbonyl resonances in the range of 180-185 ppm (Figure 1A and S2). In the single crystal X-ray diffraction structure of the natural abundance MSC, the carboxylate ligands are in a low symmetry environment, and so 51 separate carboxylate carbon resonances would be expected in a static ligand environment.[45] The room temperature spectrum of *$^{13}$C*-MSC is consistent with this interpretation, with expected line-broadening and coincidental overlap taken into consideration. Cooling the sample to -35 °C resulted in a sharpening of the peaks in the same spectral range. Raising the temperature of *$^{13}$C*-MSC to 80 °C resulted in peak broadening and coalescence of the carboxylate resonances, indicating that ligand exchange is occurring at these temperatures. Cooling the sample back to room temperature re-establishes the static ligand environment without evidence for cluster degradation. This variable-temperature $^{13}$C NMR spectroscopic monitoring contrasts with the $^{31}$P NMR spectra of myristate-ligated MSCs (see Figure 4C from reference 43), which only exhibits slight temperature-dependent shifts (but no peak broadening or coalescence), indicating the $^{31}$P environments are not in chemical exchange over the same temperature. Variable temperature in-situ UV-Vis absorbance data of $In_{37}P_{20}(O_2CCH_2Ph)_{51}$ (Figure 1B) is consistent with the $^{31}$P NMR spectra, where increasing the temperature from 25 °C to 110 °C resulted in a slight and reversible thermally-induced shift in the excitonic feature of the cluster (Figure S3). This behavior is consistent with Varshni behavior and indicates that the electronic structure and molecular orbital alignment of the cluster does not change under these conditions.[47] Taken together, these three sets of variable temperature data, $^{13}$C NMR, $^{31}$P NMR and in-situ UV-Vis, present a dynamic investigation into both the surface and core physical and electronic environments. The $^{31}$P NMR and in-situ UV-Vis absorbance data suggest at temperatures less than 100 °C, the cluster core remains intact, while the $^{13}$C NMR spectra indicate that by 80 °C, the surface carboxylates are exchanging in an intramolecular fashion.

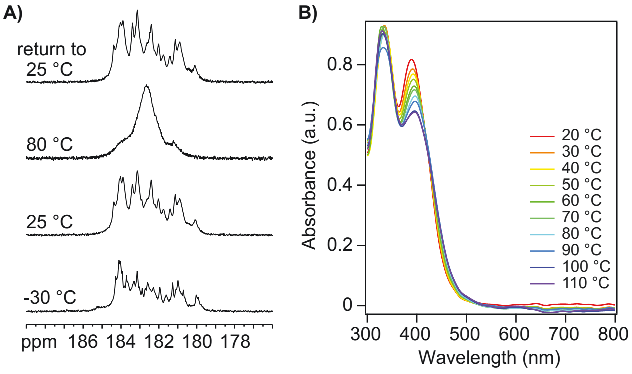

Figure 1. A) Variable temperature $^{13}$C NMR spectra (toluene-*$d_8$*, 176 MHz) of *$^{13}$C*-MSC. B) In-situ UV-Vis spectra of $In_{37}P_{20}(O_2CCH_2Ph)_{51}$ in toluene from 20 °C to 100 °C.

Next, the interactions between the cluster and exogenous additives were examined. Both phenylacetic acid and indium phenylacetate were chosen, since these species are directly relevant to the synthesis and surface chemistry of both the MSC and InP QDs. To observe surface acid exchange, increasing equivalents of isotopically enriched phenylacetic acid, $PhCH_2{}^{13}CO_2H$, were added to the natural abundance MSC, $In_{37}P_{20}(O_2CCH_2Ph)_{51}$, at room temperature. In this experiment, the only carbonyl resonances observed, either in the form of free acid or coordinated carboxylate, would arise from exogenous isotopically labeled acid, not from unlabeled native surface carboxylate ligand. If the free acid exchanges with the cluster surface, then only carboxylate resonances between 180-185 ppm would be observed. If there is no exchange with the surface at this temperature and concentration, then only free acid ($\delta = 178.80$ ppm at 25 °C) would be observed. In this experiment, upon room temperature addition of 1 equivalent of $PhCH_2{}^{13}CO_2H$ to the natural abundance MSC, the $^{13}C$ NMR spectrum (Figure 2A, bottom spectrum) reveals non-selective incorporation onto the cluster surface. While this experiment is not able to discern a kinetic selectivity in the incorporation of the exogenous acid, it does indicate that rapid exchange with surface carboxylate and exogenous labeled acid does occur, even at one equivalent of acid relative to cluster and at room temperature. Increasing the concentration of acid results in continued incorporation and the appearance of a broadened, upfield resonance corresponding to free acid that is in dynamic equilibrium with the cluster surface.

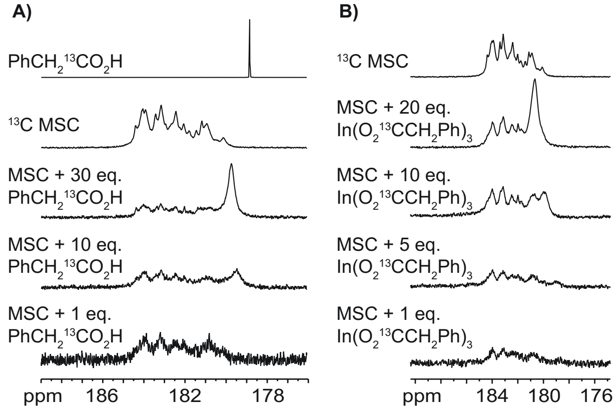

Figure 2. A) Room temperature $^{13}C$ NMR spectra (toluene-$d_8$, 176 MHz) of $In_{37}P_{20}(O_2CCH_2Ph)_{51}$ with increasing equivalents of $PhCH_2{}^{13}CO_2H$. A spectrum of authentic *$^{13}C$*-MSC is included as the topmost spectrum. B) Room temperature $^{13}C$ NMR spectra (toluene-$D_8$, 176 MHz) of $In_{37}P_{20}(O_2CCH_2Ph)_{51}$ with increasing equivalents of $In(O_2{}^{13}CCH_2Ph)_3$. A spectrum of authentic *$^{13}C$*-MSC is included as the topmost spectrum.

Analogous experiments were performed with adding increasing equivalents of isotopically labelled $In(O_2{}^{13}CCH_2Ph)_3$ to a solution of natural abundance $In_{37}P_{20}(O_2CCH_2Ph)_{51}$ (Figure 2B). Similar to the experiment with isotopically labelled phenylacetic acid, the only carboxylate carbon resonances observed in this reaction are derived from the indium carboxylate species. Upon addition of low (1-5) equivalents of indium carboxylate relative to MSC, isotopic scrambling is observed into the MSC. At 10 and 20 equivalents of indium carboxylate, a separate, broad resonance is observed, indicating saturation and free indium carboxylate in solution and exchange with the cluster. The low solubility of $In(O_2{}^{13}CCH_2Ph)_3$ precludes further analysis, but follow up studies were conducted in $CDCl_3$, with similar results (see Figure S5).

These experiments suggest that acid-induced exchange can occur at low temperatures and might be the first step in cluster dissociation during the formation of larger nanomaterials, via $k^2$-$k^1$ ligand binding interconversion or other mechanisms. In cases where the exogenous acid concentration is high, surface carboxylate exchange occurs to a greater extent, which may facilitate the total dissolution of the cluster to monomer species, consistent with recent calculations on the surface-dependent reactivity of cluster dissociation processes.[48] The additional exogenous acid (or indium carboxylate) present may also stabilize soluble monomer species in solution (e.g., through H-bonding or L- or Z-type ligand association), which would increase equilibrium constants in the cluster-to-monomer dissociation depicted in Scheme 1.

## Part 2. MSC evolution to QDs.

Having investigated the dynamics of native clusters in the presence and absence of carboxylic acid and indium carboxylate, we next sought to use in-situ spectroscopic methods to study the conversion of MSCs as single source precursors to InP QDs. We hypothesized that this process involves a complex dissolution mechanism that can be accelerated by the addition of carboxylate based on the NMR experiments presented in Part 1. To test this hypothesis we examined the conversion of myristate-ligated clusters to QDs as a function of temperature, concentration, and additive (myristic acid or indium myristate) using in situ UV-Vis spectroscopy with a fiber optic dip-probe. The results that we will present are consistent with the multiphase mechanism presented in Scheme 2 as discussed below. This proposed mechanism adds a necessary layer of complexity to the simplified reaction pathways presented in Scheme 1.

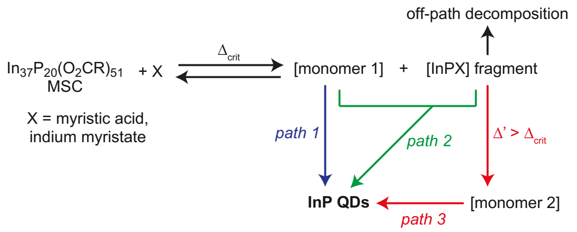

**Scheme 2. Proposed competing pathways for MSC conversion to InP QDs are dependent on temperature and additive. $\Delta_{crit}$ (130-150 °C) signifies the lowest temperature at which clusters give rise to QDs. At this temperature, significant non-productive decomposition is observed. At higher temperatures ($\Delta'$, >200 °C) full conversion to QDs occurs.**

Cluster conversion was first examined at a variety of temperatures from 150 °C to 300 °C. The intensity at 500 nm will be used as an indication of the aggregate growth of InP nanomaterials from MSCs, since there is little residual absorption from the MSC starting material at that energy, while the larger nanocrystal products do adsorb there (Figure 3A). The intensity changes at 500 nm as a function of time are plotted in Figure 3B (see Figure S6 for fits in the linear growth region). Specifically, at 150 °C, product growth continues for more than eight hours before the absorbance intensity increase at 500 nm halts (see Figure S7, S8). At ≥200 °C, the growth of product is complete within 20 minutes, with a plateau in the absorption at 500 nm near 0.2 absorbance units, and a second growth phase is observed at longer times. Based on the solution properties and TEM analysis we propose that this second distinct phase is consistent with aging of the quantum dots and a concomitant loss of colloidal stability (Figures S9, S10). At each temperature, the product growth depicted in Figure 3B can be approximated as a linear function at early time points. The lowest energy excitonic feature (LEET) of the final product at temperatures from 150-300 °C ranges from 550-650 nm, and at lower temperatures there exists a higher degree of polydispersity as indicated by the FWHM of the lowest energy electronic transition (Figure 3C). As expected, the final product synthesized at 250 °C and 300 °C exhibit a narrower absorbance feature consistent with lower polydispersity, similar to the previously reported synthesis of InP QDs from MSCs via hot-injection at 400 °C.[43]

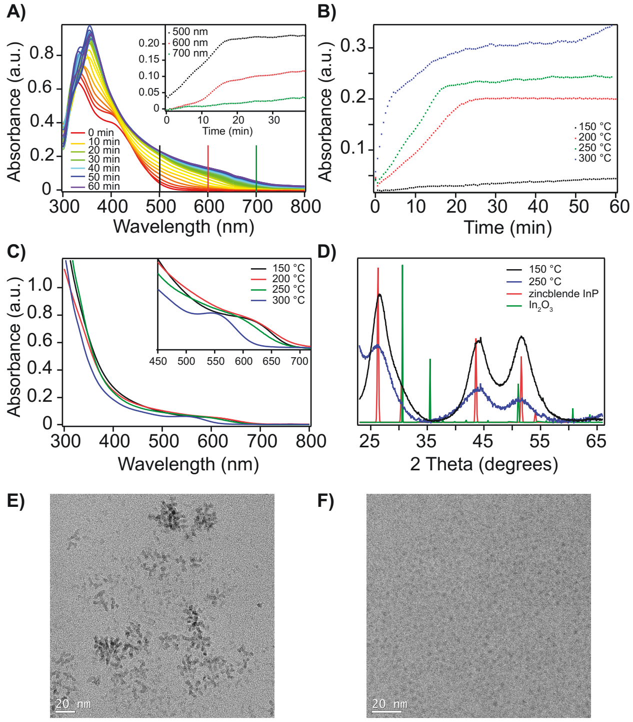

Figure 3. A) In-situ UV-Vis spectra of the conversion of InP MSCs to QDs at 250 °C over the course of 60 min. Vertical markers indicate the wavelengths at which the intensity change is depicted in the inset. B) Intensity change in the 500 nm absorbance during the evolution of InP MSC at different temperatures. C) Final absorbance spectra of the InP products. (D) Powder X-Ray Diffraction data from MSC evolution at 150 °C and 250 °C compared to bulk pattern of zincblende InP (pdf no. 01-073-1983 ICSD) and $In_2O_3$ (pdf no. 01-071-2194 ICSD). (E) Transmission electron microscopy images showing agglomerates synthesized from MSCs at 150 °C. (F) TEM images showing spherical particles synthesized from MSCs at 250 ° with an average diameter of 2.6 +/- 0.5 nm for 315 particles measured.

Representative Transmission Electron Microscopy (TEM) images of the nanomaterials synthesized at 150 °C and 250 °C are depicted in Figure 3E and 3F. Powder X-ray diffraction indicates that in both temperature regimes, zincblende InP particles are formed (Figure 3D, S11). Lattice fringe analysis revealed lattice fringes at 0.30 nm, consistent with the (200) plane of zincblende InP (Figure S12).[49] The nanoparticles synthesized at 150 °C have no uniform structure and are best described as agglomerates, whereas the morphology of the material grown at 250 °C and above shows enhanced crystallinity and is best described as spherical with an average diameter of 2.6 +/- 0.5 nm. $In_2O_3$ is a byproduct of excess indium carboxylate decomposition in some of these reactions, but separation and isolation of the InP is facile using gel permeation chromatography. The particle domain size, as determined using the Scherrer equation with the (220) peak centered at 44° 2θ, is about 3-4 nm in each case (see SI).

The differences in cluster evolution at different temperatures was also monitored by $^{31}$P NMR spectroscopy. We hypothesized that the slow and inconsistent conversion at 150 °C was due to competing rates of partial and complete MSC dissolution. To test this hypothesis, a sample of InP was heated at 130 °C for 30 hr. This temperature is low enough to limit nucleation but high enough that the MSC is not stable and slowly releases monomer (see Figure S13 for the UV-Vis time course of this reaction). The $^{31}$P NMR spectrum of the original MSC and the dissolved material is presented in Figure 4A. Thermolysis of the MSC at 130 °C resulted in a broadening and decrease in intensity of the cluster resonances (ranging from -150 to -250 ppm) along with the appearance of upfield resonances in the range of 0-100 ppm, which we attribute to products of monomer release. In the absence of sufficient thermal energy to promote crystallization, these monomers decompose non-selectively, with phosphorus oxidation a likely outcome.[50,51] This hypothesis is reinforced by powder X-ray diffraction analysis of the heated MSC sample, which indicated a non-crystalline material is formed from prolonged thermolysis at 130 °C (see Figure S14).

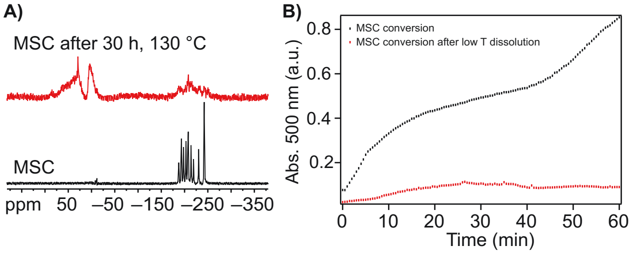

Figure 4. (A) $^{31}$P NMR (*$C_6D_6$,* 202 Hz) of $In_{37}P_{20}(\text{myristate})_{51}$ before (bottom, black) and after (top, red) treating at 130 °C for 30 hours. (B) In-situ absorbance intensity change (500 nm) over time upon treating these two samples at 250 °C via hot-injection.

Upon subjecting a sample of un-treated MSC and MSC thermolyzed at 130 °C for 72 hr to nanoparticle growth conditions at 250 °C, different profiles were observed for the two samples by UV-Vis spectroscopy (Figure 4B, Figures S15 and S16). Even though the same amount of MSC was used in both experiments, the pre-treated MSC sample that contained upfield $^{31}$P NMR resonances nucleated at a different rate and produced less semiconductor material than the un-treated MSC sample. These experiments suggest that the pre-treatment of the MSC at temperatures below the nucleation temperature leads to cluster dissolution that does not result in a monomer reservoir for nucleation. Thus, cluster conversion at lower temperatures is adversely impacted by non-productive cluster degradation.

Corroborating these findings is solid state thermogravimetric analysis (TGA) and differential scanning calorimetry (DSC) experiments performed on the clusters (see Figures S17-19). The DSC thermogram indicates that a significant endothermic event occurs in the temperature range of 115-130 °C, which we attribute to cluster melting. This process is irreversible, and upon cooling back to room temperature, an exothermic crystallization event is observed in the range of 110-90 °C. This accords well with previous observations on the thermal stability of the MSC and on the thermal decomposition reaction observed here (Figure 4). In the DSC thermogram, a smaller endothermic feature observed at 66 °C is attributed to the surface ligand rearrangement observed in the $^{13}$C NMR experiments in Figure 1. In a temperature cycling experiment, passing between the range of 35-75 °C three times had no effect on the larger, higher temperature endothermic process.

Having determined that InP MSCs are competent precursors for QD synthesis above 200 °C, we next sought to evaluate the concentration dependence of the cluster evolution at a single temperature. Monitoring the growth rate of product formation at 250 °C as a function of concentration (0.030 mM, 0.061 mM, and 0.182 mM) revealed that the rate of product formation increases as a function of initial MSC concentration. This observation indicates that the rate law of product formation is first order in MSC (Figure 5, Figure S20), despite the linear increase in absorbance intensity over the course of the reaction. A similar trend is observed when cluster evolution is monitored at 300 °C at different concentrations (see Figure S21). These observations rule out rate-limiting cluster aggregation and are consistent with our proposed dissolution mechanism.

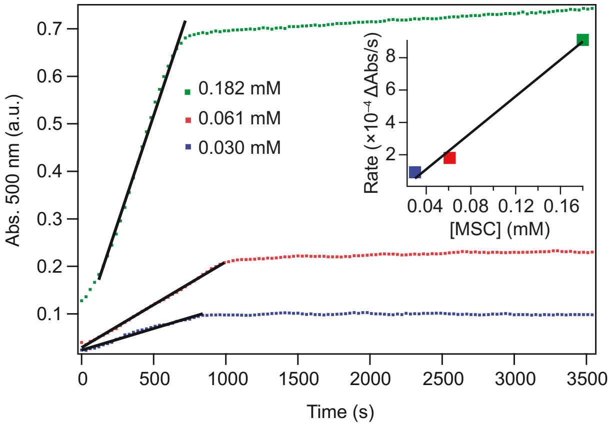

Figure 5. Intensity change in the 500 nm absorbance during the evolution of InP MSC at different concentrations at 250 °C. Inset: rate of change in intensity at 500 nm plotted as a function of initial MSC concentration. The linear fit in the inset is y = 0.00564x – 0.00012, $R^2$ = 0.9904.

The final component of our kinetics analysis involved investigation of cluster evolution in the presence of exogenous ligands, which may impact the nucleation and growth kinetics in a number of ways. For example, we have previously shown that addition of primary amines to the MSC results in site-specific ligation and rapid exchange.[52] At higher temperatures, this ligand binding influences the rate of MSC dissolution and/or the monomer reactivity.[53] Furthermore, certain exogenous additives have the potential to influence equilibria between monomers and other aggregates. To study that effect, the first additive studied was indium myristate, $In(MA)_3$, which serves as a Z-type ligand on the surface of the MSC (and presumably the QDs), and whose presence would influence Le Chatelier dynamics in the equilibria between cluster and monomer species by perturbing the cluster dissolution process. Analogous experiments were then conducted with myristic acid, which can act as both an L-type ligand by binding through an oxygen lone pair, or through X-type binding via carboxylate exchange.

In a typical modification to the experiment previously described, a solution of indium myristate was added to the reaction solution prior to MSC addition in such a manner that the overall reaction volume (20 mL) remained constant at different equivalents of indium myristate. The rates of product growth as a function of $In(MA)_3$ concentration relative to initial MSC concentration and temperature are listed in Table 1. Similar to previous experiments, a temperature-dependent rate increase is observed in each case. At lower temperatures (150 and 200 °C), the rate of product formation increases at greater equivalents of indium myristate (Table 1). At 250 °C, the effect is more pronounced, with the rate increasing by a factor of 10 when going from 0 eq. to 50 eq. of indium myristate relative to the initial MSC concentration. The final product absorbances show some variation at 150 °C indicating that as the indium myristate concentration increases, the particle size also increases (Figure S24). On the other hand, at 200 °C and 250 °C, the absorbance features are similar from 0 to 50 eq. of added indium myristate (Figure S25 and S27).

| eq. $In(MA)_3$ | growth rate at 150 °C | growth rate at 200 °C | growth rate at 250 °C |
|---|---|---|---|
| 0 | $3.50 \times 10^{-6}$ | $6.07 \times 10^{-5}$ | $1.80 \times 10^{-4}$ |
| 10 | $3.83 \times 10^{-6}$ | $9.38 \times 10^{-5}$ | $6.37 \times 10^{-4}$ |
| 20 | $6.17 \times 10^{-6}$ | $1.34 \times 10^{-4}$ | $8.03 \times 10^{-4}$ |
| 50 | $1.13 \times 10^{-5}$ | $1.31 \times 10^{-4}$ | $1.80 \times 10^{-3}$ |

**Table 1. MSC growth rate at different temperatures and equivalents of indium myristate ($\Delta_{abs}$500 nm/s).**

This rate increase as a function of increasing concentration of indium myristate stands in contrast to previous examples of MSC evolution to QDs where the presence of exogenous surface ligands *slows* the conversion to larger nanomaterials.[13] Indeed, considering Le Chatelier arguments as in the mechanism depicted in Scheme 1, the addition of indium myristate should perturb the equilibrium between MSCs and monomers to favor the reactants (MSCs), not the products, which include [InP] monomers and indium carboxylate. The rate increase associated with the presence of indium myristate could suggest that monomer species are stabilized by the presence of carboxylate. Alternatively, the Lewis acid character of the indium myristate could serve to remove the carboxylate ligands from the MSC surface, promoting the cluster dissolution and re-nucleation.

To examine these possibilities, the MSC evolution was measured in the presence of myristic acid, a Brønsted acid. The kinetics and the final product absorbance for myristic acid and indium myristate were compared (see Figures S23-S28). Adding increasing equivalents of myristic acid resulted in a similar rate increase of MSC evolution relative to no exogenous additive, and at 50 eq. of myristic acid relative to the initial MSC concentration, the growth rate was approximately half than with 50 eq. of indium myristate. This rate enhancement suggests that simple protic acids are also effective at perturbing the surface structure, enabling MSC dissolution of re-nucleation to larger QDs. Furthermore, the difference in the rate enhancement points to carboxylate as being an important operator in altering the reaction kinetics.

The comparison of the rate increase at different temperatures and different additive concentrations presents a contrast in reaction effects: at low temperatures (150 °C), the presence of increasing concentrations of additive has a pronounced effect on the final product distribution (Figure S23, S24), but little effect on the growth rate (Figure S30 and Table 1), whereas at higher reaction temperatures (250 °C and higher), the presence of increasing concentrations of additive has little effect on the product distribution (Figure S26, S27). This evidence suggests multiple reaction pathways operative as depicted in Scheme 2.

The dissolution of clusters to monomers involves a multistep process of dissociation of indium myristate and monomer species from the cluster. At temperatures at or below 150 °C this process is slow and incomplete, allowing monomer decomposition to compete with InP QD crystallization. At higher temperatures, the reaction rate is accordingly faster, bypassing the monomer decomposition route and enabling the formation of stable and soluble monomer species that nucleate to form QDs with high yield.

The addition of exogenous indium myristate or myristic acid during particle growth adds additional complexity. We propose that these additives increase the overall rate of InP QD formation by activating the InP MSC and fragment clusters toward dissolution, consistent with the NMR studies presented in Part I of this report. Carboxylate additives may also promote the stabilization of new monomer species responsible for particle growth. This effect is especially pronounced at lower temperatures, where lower available monomer results in the formation of larger, more polydisperse InP QDs. At higher temperatures, monomer generation is faster, and so the presence of carboxylate does not appreciably change the monomer concentration and thus the particle size is largely invariant as a function of added myristic acid or indium myristate.

## CONCLUSIONS

In conclusion, we have examined the conversion mechanism of InP MSCs to QDs using a combination of in-situ spectroscopic methods. The effects of temperature, concentration, and exogenous ligand on the growth rates and final product particle size were explored. These nucleation experiments were compared to NMR studies on an isotopically enriched $^{13}C$-MSC, in which both intramolecular and intermolecular ligand exchange was demonstrated to be facile, even at low temperatures when added carboxylate is present. Taken together, these findings indicate that while MSCs are competent single source precursors for InP QD synthesis, their dissolution is complex, releasing multiple monomer species with varying reactivities. This model of monomer release and cluster dissolution is consistent with first-principles calculations indicating that elementary growth processes involving carboxylate and indium dissociation are all highly surface-dependent.[48] This process is further altered by the addition of exogenous myristic acid or indium myristate, which promote monomer generation in a temperature-dependent manner.

These results contribute to our growing knowledge of the nonclassical nucleation and growth of colloidal materials and highlight the importance of considering the existence of differing monomer species as a function of reaction conditions. Especially in the case of more covalent materials like InP, the competing formation and differing reactivities of various monomer species is likely to play a central role in our ability to synthetically tailor mechanisms and thereby control product outcomes.

## EXPERIMENTAL SECTION

All glassware was dried in a 160 °C oven overnight prior to use. All reactions, unless otherwise noted, were run under an inert atmosphere of nitrogen using a glovebox or using standard Schlenk techniques. *Warning: $P(SiMe_3)_3$ is pyrophoric, extremely reactive, and should be handled with caution.* Indium acetate (99.99%), myristic acid (99%), phenylacetic acid (99%), benzylmagnesium chloride (1 M in 2-methyl-THF) were purchased from Sigma-Aldrich Chemical Co. and used without further purification. Bio-Beads S-X1 were purchased from Bio-Rad Laboratories. All solvents, including 1-ODE, toluene, pentane, ethyl acetate, and acetonitrile, were purchased from Sigma-Aldrich Chemical Co., dried over $CaH_2$, distilled, and stored over 4 Å molecular sieves in a nitrogen-filled glovebox. $C_6D_6$ and toluene-$d_8$ were purchased from Cambridge Isotope Laboratories and were similarly dried and stored. $^{13}CO_2$ (13C, 99%) was purchased from Cambridge Isotope Laboratories in a 1 L break seal flask. $P(SiMe_3)_3$ was prepared following literature procedures.[54]

$^{31}P$ NMR spectra were collected on a 700 MHz Bruker Avance spectrometer. UV–vis spectra were collected on a Cary 5000 spectrophotometer from Agilent or in situ with an Ocean Optics TI300-Series absorbance dip probe. Data collected from the dip probe were smoothed in Igor Pro with binomial smoothing algorithms. TEM images were collected on an FEI Tecnai G2 F20 microscope using an ultrathin carbon film on holey carbon purchased from Ted Pella Inc. Powder X-Ray Diffraction was collected with a Bruker D8 Discover with IμS 2-D XRD system. Thermogravimetric Analysis was conducted with a TA TGA-Q50, with a ramp rate of 10 °C / min. Differential Scanning Calorimetry was conducted with TA DSC-Q20 with a ramp rate of 10 °C / min.

Representative in-situ monitoring of cluster evolution.

An oven-dried 4 neck flask equipped with a stir bar, Schlenk line adapter, thermowell, septum, and dip-probe adapter was dried on the Schlenk line. To the flask was added 1-ODE and a solution of the desired additive in 1-ODE such that the total volume is 19 mL. The flask was heated to the desired temperature under $N_2$, at which point the dip-probe was calibrated using the Ocean View software. The baseline spectra was collected for use in data analysis later. A 20.0 mg ($1.21 \times 10^{-3}$ mmol) sample of clusters was dissolved in 1 mL of 1-ODE via sonication and rapidly injected into the reaction flask such that data collection began as soon as the sample became homogenized. Spectra were collected every 30 s during the reaction. Upon completion of the reaction, the reaction contents were transferred to the glovebox for purification following solvent distillation. The raw in-situ UV-Vis data was opened in Igor Pro (v 6.02A) and subjected to a binomial smoothing factor of 1000. The baseline spectrum was subtracted from all subsequent spectra, and the intensity at specific wavelengths was plotted as a function of time.

Synthesis of $PhCH_2{}^{13}CO_2H$. Following a modified literature prep,[55] 50 mL of benzylmagnesium chloride (1.0 M in 2-Me-THF) and 50 ml of THF were introduced into an oven dried 250 mL 3-neck round bottom flask equipped with a Schlenk adapter, hose adapter, rubber septum, and stir bar. The $^{13}CO_2$ glass bulb (1.90 L, 40.9 mmol) was assembled via the hose adapter. The reaction flask was cooled with liquid nitrogen, and the system was evacuated and left under static vacuum. The break-seal flask was broken, allowing the $^{13}CO_2$ to condense in the reaction flask. The reaction flask was warmed to -76 °C with a dry ice/acetone bath for 1 hour and then to room temperature for 8 hr. The reaction flask was cooled with an ice water bath and methanol was slowly added dropwise to quench the remaining benzylmagnesium chloride. Aqueous 1 M HCl was added until the pH was 2. The reaction mixture was extracted with $Et_2O$ (3 x 20 ml). The organic fractions were combined, washed with brine, dried over $Na_2SO_4$, filtered and the solvent removed via rotatory evaporation. The crude product mixture was dissolved in minimal dichloromethane and pentane was layered on top. After standing for 12 hours at 0 °C, white crystals were collected and dried, affording 5.15 g (92% yield). The product $^1H$ and $^{13}C$ NMR spectra matched literature reports.[56] $^1H$ NMR (700 MHz, $CDCl_3$, 23 °C): 11.4 (br s, 1H, $^{13}CO_2H$), 7.36-7.27 (overlapping m, 5H, phenyl-$CH$), 3.66 (d, $^2J_{CH} = 7.74$ Hz, 2H, $CH_2$). $^1H$ NMR (700 MHz, tol-$d_8$, 23 °C): 12.1 (br s, 1H, $^{13}CO_2H$), 7.06-7.01 (m, 2H, phenyl $CH$), 7.01-6.97 (overlapping m, 3H, phenyl $CH$), 3.16 (d, $^2J_{CH} = 7.73$ Hz, 2H, $CH_2$). $^{13}C$ NMR (176 MHz, tol-$d_8$, 23 °C): 178.77 (s, $^{13}CO_2H$), 134.13 (d, $^2J_{CC} = 2.94$ Hz, phenyl $C$), 129.99

(d, ${}^3J_{CC}$ = 1.84 Hz, phenyl *C*H), 129.05 (s, phenyl *C*H), 127.69 (s, phenyl *C*H), 41.40 (d, ${}^1J_{CC}$ = 55.64 Hz).

Synthesis of $In_{37}P_{20}(O_2{}^{13}CCH_2Ph)_{51}$. This was carried out with $PhCH_2{}^{13}CO_2H$ in place of natural abundance phenylacetic acid following the literature preparation.[43,45]

## ASSOCIATED CONTENT

### Supporting Information

The Supporting Information is available free of charge on the ACS Publications website.

Additional details regarding spectroscopic characterization, including Figures S1-S28, kinetic analysis and Scherrer analysis.

## AUTHOR INFORMATION

### Corresponding Author

* cossairt@uw.edu

### ORCID

Max R. Friedfeld: 0000-0001-5693-3705
Brandi M. Cossairt: 0000-0002-9891-3259

### Author Contributions

The manuscript was written through contributions of all authors.

### Funding Sources

David and Lucile Packard Foundation, Mary Gates Research Foundation, Washington Research Foundation, National Science Foundation (CHE- 1552164).

### Notes

The authors declare no competing financial interest.

## ACKNOWLEDGMENT

We gratefully acknowledge the David and Lucile Packard Foundation and the Washington Research Foundation (M.R.F.), the Mary Gates Research Foundation (D.A.J.), and the National Science Foundation (B.M.C. grant CHE- 1552164) for financial support of this work. Dr. Jennifer L. Stein is gratefully acknowledged for stimulating discussions influencing this work.

## ABBREVIATIONS

1-ODE, 1-octadecene; FWHM, full-width at half-maximum; $In(MA)_3$, indium myristate; LEET, lowest energy excitation transition; MA, myristate, MAH, myristic acid; MSC, magic-sized cluster; QD, quantum dot; SAXS, small-angle X-ray scattering; TEM, transmission electron microscopy; UV-Vis, ultraviolet-visible spectroscopy; WAXS, wide-angle X-ray scattering; XRD, powder X-ray diffraction.

## REFERENCES

(1) LaMer, V. K.; Dinegar, R. H. Theory, Production and Mechanism of Formation of Monodispersed Hydrosols. *J. Am. Chem. Soc.* **1950**, *72*, 4847–4854.

(2) Chu, D. B. K.; Owen, J. S.; Peters, B. Nucleation and Growth Kinetics from LaMer Burst Data. *J. Phys. Chem. A* **2017**, *121*, 7511–7517.

(3) Wall, M. A.; Cossairt, B. M.; Liu, J. T. C. Reaction-Driven Nucleation Theory. *J. Phys. Chem. C* **2018**, *122*, 9671–9679.

(4) Thanh, N. T. K.; Maclean, N.; Mahiddine, S. Mechanisms of Nucleation and Growth of Nanoparticles in Solution. *Chem. Rev.* **2014**, *114*, 7610–7630.

(5) Friedfeld, M. R.; Stein, J. L.; Cossairt, B. M. Main-Group-Semiconductor Cluster Molecules as Synthetic Intermediates to Nanostructures. *Inorg. Chem.* **2017**, *56*, 8689–8697.

(6) Kudera, S.; Zanella, M.; Giannini, C.; Rizzo, A.; Li, Y.; Gigli, G.; Cingolani, R.; Ciccarella, G.; Spahl, W.; Parak, W. J.; et al. Sequential Growth of Magic-Size CdSe Nanocrystals. *Adv. Mater.* **2007**, *19*, 548–552.

(7) Beecher, A. N.; Yang, X.; Palmer, J. H.; LaGrassa, A. L.; Juhas, P.; Billinge, S. J. L.; Owen, J. S. Atomic Structures and Gram Scale Synthesis of Three Tetrahedral Quantum Dots. *J. Am. Chem. Soc.* **2014**, *136*, 10645–10653.

(8) Groeneveld Esther; van Berkum Susanne; Meijerink Andries; de Mello Donegá Celso. Growth and Stability of ZnTe Magic-Size Nanocrystals. *Small* **2011**, *7*, 1247–1256.

(9) Schmelzer, J. W. P.; Abyzov, A. S. How Do Crystals Nucleate and Grow: Ostwald's Rule of Stages and Beyond. In *Thermal Physics and Thermal Analysis*; Hot Topics in Thermal Analysis and Calorimetry; Springer, Cham, 2017; pp 195–211.

(10) Dagtepe, P.; Chikan, V. Quantized Ostwald Ripening of Colloidal Nanoparticles. *J. Phys. Chem. C* **2010**, *114*, 16263–16269.

(11) Dagtepe, P.; Chikan, V.; Jasinski, J.; Leppert, V. J. Quantized Growth of CdTe Quantum Dots; Observation of Magic-Sized CdTe Quantum Dots. *J. Phys. Chem. C* **2007**, *111*, 14977–14983.

(12) Evans, C. M.; Love, A. M.; Weiss, E. A. Surfactant-Controlled Polymerization of Semiconductor Clusters to Quantum Dots through Competing Step-Growth and Living Chain-Growth Mechanisms. *J. Am. Chem. Soc.* **2012**, *134*, 17298–17305.

(13) Jiang, Z.-J.; Kelley, D. F. Role of Magic-Sized Clusters in the Synthesis of CdSe Nanorods. *ACS Nano* **2010**, *4*, 1561–1572.

(14) Newton, J. C.; Ramasamy, K.; Mandal, M.; Joshi, G. K.; Kumbhar, A.; Sardar, R. Low-Temperature Synthesis of Magic-Sized CdSe Nanoclusters: Influence of Ligands on Nanocluster Growth and Photophysical Properties. *J. Phys. Chem. C* **2012**, *116*, 4380–4389.

(15) Ouyang, J.; Zaman, M. B.; Yan, F. J.; Johnston, D.; Li, G.; Wu, X.; Leek, D.; Ratcliffe, C. I.; Ripmeester, J. A.; Yu, K. Multiple Families of Magic-Sized CdSe Nanocrystals with Strong Bandgap Photoluminescence via Noninjection One-Pot Syntheses. *J. Phys. Chem. C* **2008**, *112*, 13805–13811.

(16) Joo, J.; Son, J. S.; Kwon, S. G.; Yu, J. H.; Hyeon, T. Low-Temperature Solution-Phase Synthesis of Quantum Well Structured CdSe Nanoribbons. *J. Am. Chem. Soc.* **2006**, *128*, 5632–5633.

(17) Liu, Y.-H.; Wang, F.; Wang, Y.; Gibbons, P. C.; Buhro, W. E. Lamellar Assembly of Cadmium Selenide Nanoclusters into Quantum Belts. *J. Am. Chem. Soc.* **2011**, *133*, 17005–17013.

(18) Tang, Z.; Kotov, N. A.; Giersig, M. Spontaneous Organization of Single CdTe Nanoparticles into Luminescent Nanowires. *Science* **2002**, *297*, 237–240.

(19) Yu, J. H.; Joo, J.; Park, H. M.; Baik, S.-I.; Kim, Y. W.; Kim, S. C.; Hyeon, T. Synthesis of Quantum-Sized Cubic ZnS Nanorods by the Oriented Attachment Mechanism. *J. Am. Chem. Soc.* **2005**, *127*, 5662–5670.

(20) Schliehe, C.; Juarez, B. H.; Pelletier, M.; Jander, S.; Greshnykh, D.; Nagel, M.; Meyer, A.; Foerster, S.; Kornowski, A.; Klinke, C.; et al. Ultrathin PbS Sheets by Two-Dimensional Oriented Attachment. *Science* **2010**, *329*, 550–553.

(21) Cho, K.-S.; Talapin, D. V.; Gaschler, W.; Murray, C. B. Designing PbSe Nanowires and Nanorings through Oriented Attachment of Nanoparticles. *J. Am. Chem. Soc.* **2005**, *127*, 7140–7147.

(22) Harrell, S. M.; McBride, J. R.; Rosenthal, S. J. Synthesis of Ultrasmall and Magic-Sized CdSe Nanocrystals. *Chem. Mater.* **2013**, *25*, 1199–1210.

(23) Wang, F.; Richards, V. N.; Shields, S. P.; Buhro, W. E. Kinetics and Mechanisms of Aggregative Nanocrystal Growth. *Chem. Mater.* **2014**, *26*, 5–21.

(24) Liu, H.; Owen, J. S.; Alivisatos, A. P. Mechanistic Study of Precursor Evolution in Colloidal Group II−VI Semiconductor Nanocrystal Synthesis. *J. Am. Chem. Soc.* **2007**, *129*, 305–312.

(25) Owen, J. S.; Chan, E. M.; Liu, H.; Alivisatos, A. P. Precursor Conversion Kinetics and the Nucleation of Cadmium Selenide Nanocrystals. *J. Am. Chem. Soc.* **2010**, *132*, 18206–18213.

(26) Qu, L.; Yu, W. W.; Peng, X. In Situ Observation of the Nucleation and Growth of CdSe Nanocrystals. *Nano Lett.* **2004**, *4*, 465–469.

(27) Reiss, P.; Carayon, S.; Bleuse, J.; Pron, A. Low Polydispersity Core/Shell Nanocrystals of CdSe/ZnSe and CdSe/ZnSe/ZnS Type: Preparation and Optical Studies. *Synthetic Metals* **2003**, *139*, 649–652.

(28) Abécassis, B.; Bouet, C.; Garnero, C.; Constantin, D.; Lequeux, N.; Ithurria, S.; Dubertret, B.; Pauw, B. R.; Pontoni, D. Real-Time in Situ Probing of High-Temperature Quantum Dots Solution Synthesis. *Nano Lett.* **2015**, *15*, 2620–2626.

(29) Lignos Ioannis; Stavrakis Stavros; Kilaj Ardita; deMello Andrew J. Millisecond-Timescale Monitoring of PbS Nanoparticle Nucleation and Growth Using Droplet-Based Microfluidics. *Small* **2015**, *11*, 4009–4017.

(30) Tiemann Michael; Weiß Özlem; Hartikainen Juha; Marlow Frank; Lindén Mika. Early Stages of ZnS Nanoparticle Growth Studied by In-Situ Stopped-Flow UV Absorption Spectroscopy. *ChemPhysChem* **2005**, , 2113–2119.

(31) León-Velázquez, M. S.; Irizarry, R.; Castro-Rosario, M. E. Nucleation and Growth of Silver Sulfide Nanoparticles. *J. Phys. Chem. C* **2010**, *114*, 5839–5849.

(32) Evans, J. E.; Jungjohann, K. L.; Browning, N. D.; Arslan, I. Controlled Growth of Nanoparticles from Solution with In Situ Liquid Transmission Electron Microscopy. *Nano Lett.* **2011**, *11*, 2809–2813.

(33) Viswanatha, R.; Amenitsch, H.; Sarma, D. D. Growth Kinetics of ZnO Nanocrystals: A Few Surprises. *J. Am. Chem. Soc.* **2007**, *129*, 4470–4475.

(34) Caetano, B. L.; Santilli, C. V.; Meneau, F.; Briois, V.; Pulcinelli, S. H. In Situ and Simultaneous UV−vis/SAXS and UV−vis/XAFS Time-Resolved Monitoring of ZnO Quantum Dots Formation and Growth. *J. Phys. Chem. C* **2011**, *115* , 4404–4412.

(35) Segets, D.; Martinez Tomalino, L.; Gradl, J.; Peukert, W. Real-Time Monitoring of the Nucleation and Growth of ZnO Nanoparticles Using an Optical Hyper-Rayleigh Scattering Method. *J. Phys. Chem. C* **2009**, *113*, 11995–12001.

(36) Wang, Y.; Wang, S.; Lu, X. In Situ Observation of the Growth of ZnO Nanostructures Using Liquid Cell Electron Microscopy. *J. Phys. Chem. C* **2018**, *122*, 875–879.

(37) Cheong, S.; Watt, J.; Ingham, B.; Toney, M. F.; Tilley, R. D. In Situ and Ex Situ Studies of Platinum Nanocrystals: Growth and Evolution in Solution. *J. Am. Chem. Soc.* **2009**, *131*, 14590–14595.

(38) Woehl, T. J.; Evans, J. E.; Arslan, I.; Ristenpart, W. D.; Browning, N. D. Direct in Situ Determination of the Mechanisms Controlling Nanoparticle Nucleation and Growth. *ACS Nano* **2012**, *6*, 8599–8610.

(39) Park, J.; Zheng, H.; Lee, W. C.; Geissler, P. L.; Rabani, E.; Alivisatos, A. P. Direct Observation of Nanoparticle Superlattice Formation by Using Liquid Cell Transmission Electron Microscopy. *ACS Nano* **2012**, *6*, 2078–2085.

(40) Li, J.; Wang, H.; Lin, L.; Fang, Q.; Peng, X. Quantitative Identification of Basic Growth Channels for Formation of Monodisperse Nanocrystals. *J. Am. Chem. Soc.* **2018**, *140*, 5474–5484.

(41) Xie, R.; Li, Z.; Peng, X. Nucleation Kinetics vs Chemical Kinetics in the Initial Formation of Semiconductor Nanocrystals. *J. Am. Chem. Soc.* **2009**, *131*, 15457–15466.

(42) Yang, X.; Zhao, D.; Leck, K. S.; Tan, S. T.; Tang, Y. X.; Zhao, J.; Demir, H. V.; Sun, X. W. Full Visible Range Covering InP/ZnS Nanocrystals with High Photometric Performance and Their Application to White Quantum Dot Light-Emitting Diodes. *Advanced Materials* **2012**, *24*, 4180–4185.

(43) Gary, D. C.; Terban, M. W.; Billinge, S. J. L.; Cossairt, B. M. Two-Step Nucleation and Growth of InP Quantum Dots via Magic-Sized Cluster Intermediates. *Chem. Mater.* **2015**, *27*, 1432–1441.

(44) Gary, D. C.; Glassy, B. A.; Cossairt, B. M. Investigation of Indium Phosphide Quantum Dot Nucleation and Growth Utilizing Triarylsilylphosphine Precursors. *Chem. Mater.* **2014**, *26*, 1734–1744.

(45) Gary, D. C.; Flowers, S. E.; Kaminsky, W.; Petrone, A.; Li, X.; Cossairt, B. M. Single-Crystal and Electronic Structure of a 1.3 Nm Indium Phosphide Nanocluster. *J. Am. Chem. Soc.* **2016**, *138*, 1510–1513.

(46) Ritchhart Andrew; Cossairt Brandi M. Templated Growth of InP Nanocrystals with a Polytwistane Structure. *Angew. Chem. Int. Ed.* **2018**, *57*, 1908–1912.

(47) Vainshtein, I. A.; Zatsepin, A. F.; Kortov, V. S. Applicability of the Empirical Varshni Relation for the Temperature Dependence of the Width of the Band Gap. *Physics of the Solid State* **1999**, *41*, 905–908.

(48) Zhao, Q.; Kulik, H. J. Electronic Structure Origins of Surface-Dependent Growth in III–V Quantum Dots. *Chem. Mater.* **2018**. https://doi.org/10.1021/acs.chemmater.8b03125.

(49) Watanabe, T.; Wada, C.; Iso, Y.; Isobe, T.; Sasaki, H. Preparation of Photostable Fluorescent InP/ZnS Quantum Dots Embedded in TMAS-Derived Silica. *ECS Journal of Solid State Science and Technology* **2017**, *6*, R75–R80.

(50) Cros-Gagneux, A.; Delpech, F.; Nayral, C.; Cornejo, A.; Coppel, Y.; Chaudret, B. Surface Chemistry of InP Quantum Dots: A Comprehensive Study. *J. Am. Chem. Soc.* **2010**, *132*, 18147–18157.

(51) Tessier, M. D.; Baquero, E. A.; Dupont, D.; Grigel, V.; Bladt, E.; Bals, S.; Coppel, Y.; Hens, Z.; Nayral, C.; Delpech, F. Interfacial Oxidation and Photoluminescence of InP-Based Core/Shell Quantum Dots. *Chem. Mater.* **2018**. https://doi.org/10.1021/acs.chemmater.8b03117.

(52) Gary, D. C.; Petrone, A.; Li, X.; Cossairt, B. M. Investigating the Role of Amine in InP Nanocrystal Synthesis: Destabilizing Cluster Intermediates by Z-Type Ligand Displacement. *Chem. Commun.* **2016**, *53*, 161–164.

(53) Allen Peter M.; Walker Brian J.; Bawendi Moungi G. Mechanistic Insights into the Formation of InP Quantum Dots. *Angew. Chem. Int. Ed.* **2009**, *49*, 760–762.

(54) Gary, D. C.; Cossairt, B. M. Role of Acid in Precursor Conversion During InP Quantum Dot Synthesis. *Chem. Mater.* **2013**, *25*, 2463–2469.

(55) Lee, C. C.; Zohdi, H. F.; Sallam, M. M. M. Hydrogen-Deuterium Exchanges in a Friedel-Crafts Reaction. *J. Org. Chem.* **1985**, *50*, 705–707.

(56) Rosca, S. I.; Stan, R.; Ungureanu, E.-M.; Stanciu, G.; Rosca, S. $^{13}$C- and D-Labelled 3-Phenylpropionic Acids; Synthesis and

Characterization by NMR and MS Spectra. *U.P.B. Sci. Bull., Series B. 70*, 77–84.

SYNOPSIS TOC (Word Style “SN_Synopsis_TOC”).

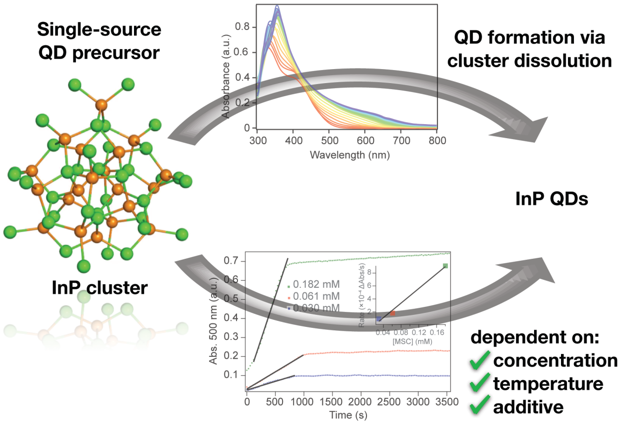

Colloidal quantum dots have emerged as an important class of emissive materials for a range of technologically relevant applications. This motivates the need to develop a detailed understanding of the mechanisms by which these nanocrystals form in order to gain predictive control over their synthesis. In this work we have studied the mechanism by which molecular InP clusters convert to quantum dots using in-situ spectroscopic methods. The effect of temperature, concentration, and added carboxylate combine to reveal a complex conversion process involving the release of multiple distinct monomer species of varying reactivity.